Uncovering inner detached resonance curves in coupled oscillators with nonlinearity

Gianluca Gatti[1]
Department of Mechanical, Energy and Management Engineering
University of Calabria
V. P. Bucci 46C, 87036, Arcavacata di Rende (CS), Italy
gianluca.gatti@unical.it

ABSTRACT

Detached resonance curves have been predicted in multi degree-of-freedom nonlinear oscillators, when subject to harmonic excitation. They appear as isolated loops of solutions in the main continuous frequency response curve and their detection may thus be hidden by numerical or experimental analysis. In this paper, an analytical approach is adopted to predict their appearance. Expressions for the amplitude-frequency equations and bifurcation curves are derived for a two degree-of-freedom system with cubic stiffness nonlinearity, and the effect of the system parameters is investigated. The interest is specifically towards the occurrence of closed detached curves appearing inside the main continuous frequency response curve, which may lead to a dramatic reduction of the amplitude of the system response. Both cases of hardening and softening stiffness characteristics are considered. The analytical findings are validated by numerical analysis.

KEYWORDS: detached resonance curve, isolated resonance curve, nonlinear vibration

[1] Corresponding author.

1 INTRODUCTION

Detached resonance curves (DRCs) appear as isolated loops of solutions in the frequency response curves (FRCs) of oscillating systems with nonlinearity. Their detection may be undisclosed either when applying classical numerical techniques or when performing sine-sweep experimental tests. An analytical approach is then convenient because it would show the effects of the main system parameters on the DRCs appearance. Furthermore, it would be helpful to predict DRCs in advance, prior to conduct any numerical or experimental analysis.

DRCs manifest as a result of multivaluedness in the FRC [1]. This means that, in case of harmonic excitation and provided the system response is predominantly harmonic at the excitation frequency, multiple solutions may appear in the steady-state amplitude responses at a single frequency. Depending on the values of the system parameters, multivaluedness can lead to closed DRCs, which can either lay inside or outside the main continuous FRC.

Analyzing the performance of a vibration absorber with a nonlinear damping characteristics attached to a linear host structure, Starosvetsky and Gendelman [2] reported theoretical prediction and numerical confirmation of outer DRCs. The same authors predicted similar features when analyzing a three degree-of freedom (DOF) nonlinear oscillating system [3]. The values of the system parameters greatly affect the appearance of these features, so that, for instance, in the two DOF experimental setup tested in [4] DRCs did not manifest. Alexander and Schilder [5] found out a family of outer DRCs for vanishing linear spring stiffness term when analyzing the performance of a nonlinear tuned mass damper with linear plus cubic stiffness nonlinearity. Detroux et al

[6] identified DRCs numerically in the forced response of a satellite structure. Kuether et al [7] studied the connection between nonlinear normal modes and isolated resonance curves appearing outside the main frequency response curve of a forced nonlinear system. A family of isolated sub-harmonic branches in the nonlinear frequency response of an oscillator with clearance was studied in [8], and outer detachments were also observed in case of impact phenomena [9]. By studying the response of a harmonically excited system consisting of coupled linear and nonlinear oscillators with hardening characteristics, Gatti and Brennan [10] predicted the appearance of either inner or outer DRCs and investigated the effect of parameters in the appearance of such features. They studied the system under the assumption of very small ratio between the mass of the attachment and that of the main structure. An experimental test was also conducted by the use of a very heavy electro-magnetic shaker and a relative light mass for the attachment [11], but the physical system parameters were not suitable to uncover a DRC experimentally. In that case, it was evident that inner DRC manifests for low values of the linear stiffness and damping in the attachment. Despite the theoretical formulation used in [10] and [11] captures physically the phenomena of DRCs, its practical application to real engineering design problems is limited by the former assumption about the mass ratio.

To the best of the author's knowledge it seems that there is no comprehensive work which clearly shows the effects of the main parameters of a nonlinear oscillating system on the appearance of such features, and the conditions and limitations for those features to emerge in the main continuous FRC. Thus, with the aim to provide a series of analytical usable expressions related to such interesting phenomenon, this paper presents

a detailed theoretical analysis on the response of a harmonically excited two DOF oscillating system with coupling nonlinear stiffness. By removing previous limitations, as the assumption of small mass ratio [11] or the assumption of a light primary suspension [12], a novel and complete closed-form solution for the amplitude-frequency response equation and detachments is derived using the harmonic balance method. Both the cases of nonlinear hardening and softening spring are considered and it is shown how this characteristics affects the occurrence of a DRC and the corresponding ranges for the values of the system parameters.

Uncovering the main mechanism underneath the appearance of DRC will help engineers to better design nonlinear system (or system expected to operate in nonlinear conditions) and thus avoiding (or exploiting) a detachment to arise in the frequency response with a consequent dramatic amplitude shift.

The theoretical approach adopted in this work can be extended to different configurations of nonlinear coupled oscillators, so as to investigate their specific dynamic behavior when subject to harmonic excitation.

2 SYSTEM DESCRIPTION AND EQUATIONS OF MOTION

The system of interest in this work is shown in Fig. 1. A primary oscillating mass m_s is connected to ground through a linear spring k_s and damper c_s and it is excited by a force f. A secondary mass m is attached to the first mass through a linear damper c_1 and a nonlinear spring, which consists of a linear, k_1, plus cubic, k_3, stiffness term.

The equations of motion of the system may be written in terms of the displacement of the primary mass, x_s, and the relative displacement between the two masses, $z = x_s - x$, where x is the displacement of the secondary mass. They are given below as

$$\begin{aligned} m_s\ddot{x}_s + c_s\dot{x}_s + k_s x_s + c_1\dot{z} + k_1 z + k_3 z^3 &= f(t) \\ m\ddot{x}_s - m\ddot{z} - c_1\dot{z} - k_1 z - k_3 z^3 &= 0 \end{aligned}, \tag{1a,b}$$

where the overdots denote differentiation respect to time t.

If the primary mass is driven by a harmonic force with constant amplitude F at each frequency ω, i.e. $f(t) = F\cos(\omega t)$, Eqs. (1a,b) can be conveniently written in non-dimensional form as

$$\begin{aligned} y_s''(1+\mu) + 2\zeta_s y_s' + y_s &= \cos(\Omega\tau) + \mu w'' \\ w'' + 2\zeta w' + \Omega_0^2 w + \gamma w^3 &= y_s'' \end{aligned}, \tag{2a,b}$$

where $y_s = x_s/x_0$, $y = x/x_0$ and $w = z/x_0$ are the non-dimensional absolute displacements of the two masses and the non-dimensional relative displacement, respectively, in which $x_0 = F/k_s$ is the static displacement of the primary mass; $\Omega = \omega/\omega_s$ is the non-dimensional frequency in which $\omega_s = \sqrt{k_s/m_s}$; $\mu = m/m_s$ is the mass ratio; $\gamma = k_3 x_0^2/\mu k_s$ is the non-dimensional nonlinear parameter; $\zeta_s = c_s/2m_s\omega_s$ and $\zeta = c_1/2m\omega_s$ are the damping ratios; $(\cdot)' = d(\cdot)/d\tau$, in which $\tau = \omega_s t$ is non-

dimensional time; and the following frequency ratio is defined $\Omega_0 = \omega_1/\omega_s$, where $\omega_1 = \sqrt{k_1/m}$.

It is interesting to note that the frequency ratio squared represents the non-dimensional linear stiffness of the attached secondary system in Eq. (2b), and it can be compared to the non-dimensional stiffness of the primary system, which is 1 in Eq. (2a). For the linear case where $\gamma = 0$, if $\Omega_0 < 1$, then the attachment suspension is softer than that of the primary oscillator, while if $\Omega_0 > 1$ it is harder. This physical observation will be of particular importance when discussing those two specific cases in conjunction with a hardening or softening nonlinearity, as reported below from Section 4 and on.

It is also observed that a change in the nonlinear parameter γ may be due to a change in the amplitude of excitation *F*, or in the cubic stiffness coefficient k_3 of the spring, or in the mass ratio μ, or in a combination of them.

3 AMPLITUDE-FREQUENCY EQUATIONS

Predictions for the steady-state solutions of the equations of motion given by Eqs. (2a,b), in terms of amplitude-frequency expressions, are found in the assumption that the response of the system is predominantly harmonic at the frequency of excitation. For this purpose, the non-dimensional absolute displacement of the primary mass and the non-dimensional relative displacement between the two masses are assumed to be in the form of $y_s \approx y_{sh}(\tau) = Y_s \cos(\Omega\tau + \varphi_s)$ and $w \approx w_h(\tau) = W\cos(\Omega\tau + \varphi)$, respectively. By then substituting these expressions into Eqs. (2a,b) and applying the harmonic balance method

to the first-order approximation, i.e. limited to the response at the excitation frequency, the following expressions are determined

$$a\gamma^2 W^6 + b\gamma W^4 + cW^2 + d = 0, \tag{3}$$

$$Y_s^2 = \frac{1 - W^4 g - W^2 h}{e}, \tag{4}$$

where

$$\begin{aligned}
a &= \frac{9}{16}, \\
b &= \frac{3}{2}\left(\Omega_0^2 - \Omega^2\right) + \Omega^4 \frac{g}{e}, \\
c &= \left(\Omega_0^2 - \Omega^2\right)^2 + 4\zeta^2\Omega^2 + \Omega^4 \frac{h}{e}, \\
d &= -\frac{\Omega^4}{e}, \\
e &= \left(1 - \Omega^2\left(1+\mu\right)\right)^2 + 4\zeta_s^2\Omega^2 \\
g &= -\frac{3}{2}\mu\left(1 - \Omega^2\left(1+\mu\right)\right) \\
h &= \Omega^4\mu^2 - 2\mu\left(1 - \Omega^2\left(1+\mu\right)\right)\left(\Omega_0^2 - \Omega^2\right) + 8\zeta\zeta_s\mu\Omega^2
\end{aligned} \tag{5a-g}$$

The amplitude of the non-dimensional absolute displacement of the secondary mass is obtained as

$$Y^2 = \left(Y_s\ \cos\left(\varphi_s\right) - W\cos\left(\varphi\ \right)\right)^2 + \left(Y_s\ \sin\left(\varphi_s\right) - W\sin\left(\varphi\ \right)\right)^2, \tag{6}$$

where the cosine and sine functions of the phases, together with some more details on the derivation of the equations reported above, are given in Appendix A.

4 BIFURCATION CURVES

In Section 3, the amplitude-frequency equations for the system non-dimensional displacements were derived. In particular, it may be noted that Eq. (3) is an implicit cubic equation in terms of W squared, Eq. (4) gives the amplitude Y_s as a function of the amplitude W, and Eq. (6) gives the amplitude Y as a function of Y_s and W. Since Eq. (3) is cubic, it may yield up to three solutions for W and thus for Y_s and Y, the type of which depends on the discriminant Δ of the cubic polynomial on the left-hand side of Eq. (3), which is given by

$$\Delta = -27\gamma^4 a^2 d^2 + \gamma^3\left(18abcd - 4b^3 d\right) + \gamma^2\left(b^2c^2 - 4c^3 a\right). \tag{7}$$

If $\Delta > 0$ then there are three distinct real roots, which correspond to three steady-state amplitudes in the FRCs (some may be unstable - stability will be discussed below in Section 5); if $\Delta < 0$ there is one real root, and a pair of complex conjugate roots, which correspond to only one real steady-state amplitude in the FRCs; if $\Delta = 0$ then two roots coincide so there are two coincident steady-state amplitude, which occur at the jump-up and jump-down frequencies in the FRCs. From the mathematical point of view, this latter condition corresponds to a so called *fold bifurcation* [4], while from a physical point of view, the *jump frequencies* are the frequencies where there is a sudden discontinuous

change of the amplitude of the response when the frequency is varied very slowly [13, 14], e.g. during a sine sweep test.

The transition between the case of a multivalued response, i.e. for $\Delta > 0$, and the case of a single-valued response, i.e. for $\Delta < 0$, is obtained by setting the discriminant in Eq. (7) to zero [13] and solving for γ to yield the following two non-null bifurcation curves in the $\Omega - \gamma$ plane

$$\gamma_{1,2} = \frac{\left(18abcd - 4b^3 d\right) \mp \sqrt{\left(18abcd - 4b^3 d\right)^2 + 108a^2 d^2 \left(b^2 c^2 - 4c^3 a\right)}}{54a^2 d^2}. \qquad \text{(8a,b)}$$

Equations (8a) and (8b) thus represent the implicit expressions for the frequencies where a jump occurs, and they are ordered so that γ_1 form Eq. (8a) is smaller than γ_2 from Eq. (8b).

For the particular case where $\zeta_s = \zeta = 0$, there will be no jump-down frequency (it will tend to an infinite value) and the bifurcation curve relative to the jump-down frequencies, γ_d, will annihilate, i.e. $\gamma_d = \gamma_1 = 0$. On the other hand, the bifurcation curve relative to the jump-up frequencies, γ_u, reduces to

$$\gamma_u\big|_{\zeta_s=\zeta=0} = \gamma_2\big|_{\zeta_s=\zeta=0} = \frac{16\left(\Omega^4 + \Omega_0^2 - \Omega^2\left(1 + \left(1+\mu\right)\Omega_0^2\right)\right)^3}{81\Omega^4\left(-1 + \left(1+\mu\right)\Omega^2\right)}. \qquad \text{(9)}$$

It will be shown later in Figs. 6-7 that for a hardening system the jump-up frequency is generally lower than the jump-down frequency, and this is because the effect of a positive nonlinearity is to generally bend the resonance frequencies to the higher frequencies. For a softening system, on the other hand, the jump-down frequency is generally lower than the jump-up frequency, and this is because the effect of a negative nonlinearity is to generally bend the resonance frequencies to the lower frequencies.

As a results, for a hardening stiffness, the bifurcation curve γ_u corresponds to γ_2 in Eq. (8b), and the bifurcation curve γ_d corresponds to γ_1 in Eq. (8a). For a softening stiffness, the bifurcation curve γ_u corresponds to γ_1 in Eq. (8a), and the bifurcation curve γ_d corresponds to γ_2 in Eq. (8b). In this latter case it is in fact $|\gamma_1| > |\gamma_2|$.

It is worth mentioning here that at a frequency where a jump occurs, the system response will be subject to a sudden discontinuous change in the amplitude of all the non-dimensional displacements *W*, Y_s and *Y*, since they are related by Eqs. (3), (4) and (6). However, since the bifurcation curves reported in Eqs. (8) were derived from Eq. (3), which gives the implicit amplitude-frequency equation of the non-dimensional relative displacement *W*, the specific type of jump (i.e. a jump-up or -down) will be related to the specific FRC of *W*. As will be shown later in Fig. 9, a jump-up in the FRC of *W* may actually turn into a jump-down in the FRC of *Y*, and this will depend on the specific values of the system parameters.

To show the effects of the system parameters on the bifurcation curves, Eqs. (8a,b) and Eq. (9) are plotted in Figs. 2-5 for different combinations of the values of Ω_0, μ, ζ_s and ζ. In the colored figures, green lines correspond to the bifurcation curves for the jump-down frequencies, magenta lines correspond to the bifurcation curves for the

jump-up frequencies, and thin solid black lines represent the bifurcation curve from Eq. (9). Furthermore, a consecutive and continuous set of solutions in the bifurcation curves will be referred to as a *branch*.

It may thus be noted from Figs. 2-5, that there could be several distinct branches in the bifurcation curves, both for those related to the jump-up frequencies, and for those related to the jump-down frequencies. For example, in Fig. 3(b), for positive values of nonlinearity and for each value of damping ζ, there is one branch of the bifurcation curve for the jump-up frequencies (magenta line) and one branch of the bifurcation curve for the jump-down frequencies (green line). On the other hand, for negative values of the nonlinearity, there are two branches of the bifurcation curve for the jump-up frequencies (magenta lines) and two branches of the bifurcation curve for the jump-down frequencies (green lines).

A branch related to the jump-up frequencies may form a closed loop together with a branch related to the jump-down frequencies. For example, in Fig. 3(b), for positive values of nonlinearity, the magenta line joins the green line at around Ω=1.5. For negative values of nonlinearity, the magenta and green branches on the lower frequencies join at around Ω=0.9, while the magenta and green branches on the higher frequencies join at around Ω=0.95 and Ω=1.5, thus forming an isolated loop.

In particular, in Fig. 2 the effect of the damping of the primary mass is shown. Figure 2(a) shows the effect of ζ_s for a value of Ω_0 less than 1, while Fig. 2(b) shows the same effect for a value of Ω_0 greater than 1. It can be observed that the effect of ζ_s is significant only for the bifurcation curve representing the jump-down frequencies, while the bifurcation curve representing the jump-up frequencies are not effected much.

Furthermore these latter curves do match very well to the bifurcation curve for the jump-up frequencies given by Eq. (9) for $\zeta_s = \zeta = 0$ (thin solid line).

A similar behavior is observed in Fig. 3, which shows the effect of the damping in the attachment, ζ.

The effect of mass ratio, μ, and of the frequency ratio, Ω_0, on the bifurcation curves is more profound, and it is shown in Fig. 4 and Fig. 5, respectively. Both the bifurcation curves representing the jump-up and jump-down frequencies are significantly affected by either the mass or the frequency ratio. However, is should be noted that, also in this case, the curves representing the jump-up frequencies match very well the approximate expression given by Eq. (9) for $\zeta_s = \zeta = 0$.

Of particular interest in this paper is the relative maximum or the relative minimum in the bifurcation curve for the jump-up frequencies, since this is related to the appearance of the inner detached resonance curve, as discussed later on in Section 6.

5 STABILITY OF THE STEADY-STATE SOLUTIONS

The stability of the steady-state solutions of Eqs. (3), (4) and (6) is calculated by applying Floquet theory as described in [15]. To this aim, disturbances $u(\tau)$ and $v(\tau)$ are introduced to the harmonic solutions $y_{sh}(\tau)$ and $w_h(\tau)$ of the equations of motions given in Eqs. (2a,b), leading to

$$\begin{aligned} y_s(\tau) &= y_{sh}(\tau) + u(\tau) \\ w(\tau) &= w_h(\tau) + v(\tau) \end{aligned} . \qquad \text{(10a,b)}$$

Substituting Eqs. (10a,b) into Eqs. (2a,b), the following linearized variational equations are obtained

$$\begin{aligned} u''(1+\mu)+2\zeta_s u'+u-\mu v''=0 \\ v''+2\zeta v'+\Omega_0^2 v+3\gamma w_h^2 v-u''=0 \end{aligned}, \tag{11a,b}$$

which admit solutions of the form [15]

$$\begin{aligned} u(\tau)=e^{\lambda\tau}\phi_u(\tau) \\ v(\tau)=e^{\lambda\tau}\phi_v(\tau) \end{aligned}, \tag{12a,b}$$

where $\phi_u(\tau)$ and $\phi_v(\tau)$ are periodic functions of period $2\pi/\Omega$.

Substituting Eqs. (12a,b) into Eqs. (11a,b) yields

$$\begin{aligned} &(1+\mu)\phi_u''+2\phi_u'\left((1+\mu)\lambda+\zeta_s\right)+\phi_u\left((1+\mu)\lambda^2+2\zeta_s\lambda+1\right)-\mu\phi_v''-2\mu\lambda\phi_v'-\mu\lambda^2\phi_v=0 \\ &\phi''+2\phi_v'\left(\lambda+\zeta\right)+\phi_v\left(\lambda^2+2\zeta\lambda+\Omega_0^2+3\gamma w_h^2\right)-\phi_u''-2\lambda\phi_u'-\lambda^2\phi_u=0 \end{aligned}, \tag{13a,b}$$

which may be solved once $\phi_u(\tau)$ and $\phi_v(\tau)$ are expanded in Fourier series to the first term as

$$\begin{aligned} \phi_u(\tau)=C_u\cos(\Omega\tau)+S_u\sin(\Omega\tau) \\ \phi_v(\tau)=C_v\cos(\Omega\tau)+S_v\sin(\Omega\tau) \end{aligned}. \tag{14a,b}$$

Substituting Eqs. (14a,b) into Eqs. (13a,b) and equating the harmonic coefficients on both sides of each equation, yields a system of four linear homogeneous algebraic equations in the unknowns C_u, S_u, C_v, S_v whose coefficient matrix is

$$\begin{bmatrix} (1+\mu)\left(\lambda^2-\Omega^2\right)+2\zeta_s\lambda+1 & 2\Omega\left((1+\mu)\lambda+\zeta_s\right) & -\mu\left(\lambda^2-\Omega^2\right) & -2\mu\lambda\Omega \\ -2\Omega\left((1+\mu)\lambda+\zeta_s\right) & (1+\mu)\left(\lambda^2-\Omega^2\right)+2\zeta_s\lambda+1 & 2\mu\lambda\Omega & -\mu\left(\lambda^2-\Omega^2\right) \\ -\left(\lambda^2-\Omega^2\right) & -2\lambda\Omega & \lambda^2-\Omega^2+2\zeta\lambda+\Omega_0^2+\frac{3}{2}\gamma W^2\left(1+\frac{1}{2}\cos(2\varphi)\right) & 2(\lambda+\zeta)\Omega-\frac{3}{4}\gamma W^2\sin(2\varphi) \\ 2\lambda\Omega & -\left(\lambda^2-\Omega^2\right) & -2(\lambda+\zeta)\Omega-\frac{3}{4}\gamma W^2\sin(2\varphi) & \lambda^2-\Omega^2+2\zeta\lambda+\Omega_0^2+\frac{3}{2}\gamma W^2\left(1-\frac{1}{2}\cos(2\varphi)\right) \end{bmatrix}. \tag{15}$$

Setting the determinant of the coefficient matrix in Eq. (15) equal to zero, an eighth-order polynomial equation is obtained in terms of the parameter λ, which can be solved numerically for specific values of the system parameters. It then follows from Eqs. (12a,b) that the harmonic solutions $y_{sh}(\tau)$ and $w_h(\tau)$, derived in Section 3, are asymptotically stable if and only if all of the eigenvalues λ lie in the left half of the complex plane, while it is unstable if at least one eigenvalue lies in the right half of the complex plane.

In the FRCs reported in this paper, stable solutions are represented by solid lines, while unstable solutions are represented by dashed lines. In particular, for the colored figures, red dashed lines indicate the existence of at least one real positive eigenvalue, and the point at which stability is lost, is associated with a fold bifurcation, as mentioned above in Section 4. Moreover, magenta dashed lines indicate the existence of only complex conjugate eigenvalues with positive real parts, and the point at which stability is lost, i.e. where the eigenvalues cross the imaginary axis, is associated with a Neimark-Sacker

bifurcations [6]. In this latter case, a quasi-periodic motion manifests in the system response.

As defined early for the bifurcation curves, a consecutive and continuous set of steady-states amplitude solutions, either stable or unstable, will also be referred to as a *branch* in the FRC.

6 FREQUENCY RESPONSE CURVES

The FRCs of the amplitudes W, Y_s and Y of the non-dimensional displacements as functions of Ω are calculated using Eqs. (3), (4) and (6), respectively, for particular values of the system parameters.

To emphasize the relationship between the bifurcation curves in the $\Omega-\gamma$ plane and the FRCs in the $\Omega-W$ plane, a three-dimensional plot involving the three variables Ω,γ,W is adopted and shown in Figs. 6 and 7. In both figures, the damping ratios are set to 0.01 and the mass ratio is set to 0.05. Figure 6 illustrates the case of a hardening nonlinearity where the frequency ratio is set to 0.2 and the nonlinearity is decreased from 0.2 in Fig. 6(a), 0.008 in Fig. 6(b) down to 0.0004 in Fig. 6(c). Figure 7 illustrates the case of a softening nonlinearity where the frequency ratio is set to 1.4 and the nonlinearity is increased from -0.06 in Fig. 7(a), -0.006 in Fig. 7(b) up to -0.0001 in Fig. 7(c).

Such a visual representation and relation between the FRC and the bifurcation curve, in a non-dimensional parameter space, was introduced in [16] to analyse the response of a harmonically excited two DOF system with a nonlinear quasi-zero stiffness oscillator with a light mass. Very recently in [6], by analysing the forced response of a cantilever beam with a nonlinear spring attached at its tip, such relation has been further extended

by numerically computing a three-dimensional bifurcation curve in a dimensional parameter space, whose projection on a specific plane is related to that considered in [16] and in this present paper.

In particular, Figs. 6 and 7 illustrate the relationship between the bifurcation curves from Eqs. (8a,b) and the FRCs form Eq. (3), for a system with hardening and softening stiffness characteristic, respectively. It is noted how any combination of γ and Ω from the area between the two bifurcation curves (the green and magenta lines in the colored figures) yields a multivalued response with three distinct real solutions for the steady-state amplitude response.

It can be also seen that a straight line, drawn for a particular value of γ, may be interpreted as the projection of the corresponding FRC on the $\Omega-\gamma$ plane. Moreover, the intersections between this straight line and the bifurcation curves give the values of the jump frequencies.

It may be noted in Fig. 6(a) that the horizontal dashed straight line for γ on the $\Omega-\gamma$ plane intersects only one branch of the bifurcation curve related to the jump-up frequencies (magenta curve) in one single point. This intersection point determines the value of the jump-up frequency. The vertical straight dashed line drawn on the $\Omega-W$ plane emphasizes this relation.

In a similar manner, in Fig. 6(b) the horizontal dashed straight line for γ on the $\Omega-\gamma$ plane intersect one branch of the bifurcation curve related the jump-up frequencies (magenta curve) in two points, and the other branch (magenta curve) in one point. They correspond to the values of the jump-up frequencies as emphasized by the vertical dashed straight lines on the $\Omega-W$ plane. It may also be noted that there is also a jump-down

frequency resulting from the intersection of the horizontal dashed straight line for γ on the $\Omega-\gamma$ plane and the bifurcation curve related to the jump-down frequencies (green curve). This intersection appears to be around $\Omega=2$. In Fig. 6(c) the horizontal dashed straight line for γ on the $\Omega-\gamma$ plane intersects each branch of the bifurcation curves only once, and this corresponds to the jump-up and jump-down frequencies as indicated in the figure.

For a softening spring characteristics a similar behaviour is shown in Figs. 7(a)-(c).

It is observed form Figs. 6(b) and 7(b), that an isolated DRC inside the main continuous FRC appears as a consequence of a double intersection of the straight line for γ on the $\Omega-\gamma$ plane with a same branch of the bifurcation curve related to the jump-up frequencies (magenta curve). And this is because an inner DRC is characterized by two consecutive jump-up frequencies. This happens when a branch of the bifurcation curve presents extrema points. Similarly an outer DRC, i.e. an isolated detachment outside the main continuous FRC, is characterized by two consecutive jump-down frequencies, and this is evident from Fig. 7(c).

For a better visualization of the FRCs of the amplitudes W, Y_s and Y, they are plotted, using Eqs. (3), (4) and (6), respectively, in Fig. 8(a)-(c) and in Fig. 9(a)-(c) for the values of the system parameters corresponding to those of Fig. 6(b) and Fig. 7(b), respectively, i.e. for the cases where an inner DRC manifests inside the continuous FRC of the relative displacement W. It can also be better observed that in the case of a softening spring there are frequency ranges where no periodic solution exists (as a quasi-periodic solution exists in this region), or where the only stable branch corresponds to that of a DRC.

Furthermore, as anticipated above in Section 4, Fig. 9(c) illustrates a case where the system parameters are such that an inner detachment in the FRC of *W*, turns into a different type of detachment in the FRC of *Y*.

The approximate analytical solutions are checked by direct numerical integration of the equations of motion given in Eqs. (2a,b). Simulations are performed until steady-state is achieved in the response and different initial conditions are used to achieve different amplitude responses in case of multivaluedness. The Fourier coefficients corresponding to the excitation frequency are extracted from the displacement time histories, and plotted as circles in the FRCs reported in Figs. 8 and 9. It is verified that the amplitudes of higher and lower harmonics never exceed 5% of the amplitude at the fundamental frequency. As can be noted from the results of the validation reported in Figs. 8 and 9, good agreement is achieved between the analytical and numerical solution of the FRCs.

7 INSIGHT INTO THE APPEARANCE OF INNER DETACHMENTS

To get a closer insight into the appearance of inner DRCs in the FRC of the relative displacement amplitude *W* of the nonlinear system considered in this paper, it is first recalled, as observed in Section 6, that the condition for an inner DRC to manifest is associated to the presence of a relative maximum or minimum in the bifurcation curve related to the jump-up frequencies. This is because an inner DRC is formed when the projection of the FRC on the $\Omega - \gamma$ plane intersects twice the same branch of the corresponding magenta bifurcation curve.

It is now convenient to start with a specific numerical case, corresponding to particular values of the system parameters, and then generalize the results.

To this purpose the bifurcation curve corresponding to the jump-up frequencies which are reported in Eq. (8) is plotted in Fig. 10 as a solid magenta line for the $\zeta_s = \zeta = 0.01$, $\Omega_0 = 1.4$ and $\mu = 0.1$. It is noted that a linear scale is now used in Fig. 10, to better emphasize the specific curve trend.

It was not possible to derive simple useful expressions for the extrema of the curves corresponding to Eq. (8), however the numerical solutions corresponding to the frequencies of the extrema points, A_2 and A_3, are reported in Table 1. Furthermore, it is observed in Fig. 10 that the bifurcation curve is not defined for all frequencies, but there could exist ranges of frequencies where it does not have real values. Each continuous portion of the bifurcation curve was earlier defined as a *branch*, so that the bifurcation curve plotted by the solid magenta line in Fig. 10 is formed by three separate branches, and the relative maximum A_2 and minimum A_3 belong to one same branch only.

To derive useful analytical expressions involving the system parameters which let an insight into the inner DRC appearance, some approximation are introduced.

A first approximation was already introduced in Section 4 by observing that the damping in the system does not affect significantly the bifurcation curve corresponding to the jump-up frequencies, as evident from Figs. 2 and 3. Equation (9) was then introduced and plotted in Figs. 2 and 3 as to show the approximation introduced by considering no damping in the system. Equation (9) is now also plotted in Fig. 10 as a dotted line and it is clearly seen that its approximation to the bifurcation curves of Eq. (8) is relatively good. It is also noted that Eq. (9) is defined for all frequencies in the frequency range plotted in Fig. 10, except for $\Omega = 1/\sqrt{1+\mu} \approx 0.953$ where it tends to infinity.

To determine the extrema points of Eq. (9), this is differentiated once respect to Ω and set to zero yielding

$$\left.\frac{\partial}{\partial\Omega}\gamma_u\right|_{\zeta_s=\zeta=0}=\frac{32\left(\Omega^4-\Omega^2\left(1+\left(1+\mu\right)\Omega_0^2\right)+\Omega_0^2\right)^2\left(3\left(1+\mu\right)\Omega^6-4\Omega^4+\Omega^2\left(1-2\left(1+\mu\right)\Omega_0^2\right)+2\Omega_0^2\right)}{81\Omega^5\left(-1+\left(1+\mu\right)\Omega^2\right)^2}=0 \tag{16}$$

It is noted that the numerator of Eq. (16) has been factorized, so that the solution to Eq. (16) may be obtained as the solutions of the two factors set to zero separately. The solutions of the first factor in the numerator of Eq. (16) are given below as

$$\Omega=\sqrt{\frac{1}{2}\left(1+\left(1+\mu\right)\Omega_0^2\pm\sqrt{-4\Omega_0^2+\left(1+\left(1+\mu\right)\Omega_0^2\right)^2}\right)},$$

whose numerical values, corresponding to the parameters used to plot Fig. 10 are about 0.922 and 1.519, and correspond, respectively, to the inflexion points B_1 and B_4 of the dotted line plotted in Fig. 10. These are also reported in Table 1.

The second factor in Eq. (16) is cubic in Ω^2 and the symbolic expressions for its solutions are not reported here since they are relatively long and thus not suitable for subsequent analysis. However the numerical values corresponding to the real positive solutions for the extrema points B_2 and B_3, as listed in Table 1, are very close to those corresponding to the bifurcation curve with no approximation for damping from Eq. (8). Points B_2 and B_3 are also plotted in Fig. 10.

Despite the unsuitability of Eq. (16) to reveal some useful expressions for the extrema in the bifurcation curve, it is interesting to note that the second factor in Eq. (16), which gives the solution for these extrema points, is cubic in Ω^2 and thus Descartes' rule of signs [17] can be applied to get an insight on the type of solutions. Since only the coefficient for Ω^2 can be either positive or negative, depending on the values of Ω_0 and μ, it results that this second factor has always one real negative root in terms of Ω^2 (corresponding to a pair of complex conjugate roots for Ω), while the type of the other two roots in terms of Ω^2 can be either real positive (corresponding to a pair of real roots for Ω) or complex conjugate (corresponding to a pair of complex conjugate roots for Ω). As a consequence, the sign of the discriminant of the cubic polynomial corresponding to the second factor in the numerator of Eq. (16) can be used to reveal the condition where extrema points exist. This discriminant is reported below as

$$\Delta^* = 4\left(1-3\mu+2\left(11+\mu\left(-44+9\mu\right)\right)\Omega_0^2-\left(1+\mu\right)^2\left(47+36\mu\right)\Omega_0^4+24\left(1+\mu\right)^4\Omega_0^6\right). \quad (17)$$

In particular, only in the case where this discriminant is positive, extrema points exist. If Eq. 17 is set to zero, an implicit function involving the parameters Ω_0 and μ is obtained, and this is plotted in Fig. 11. On this curve the discriminant of Eq. (17) is zero, outside this curve it is positive, and inside it is negative. This latter region is grey-shaded in Fig. 11 to show that for values of Ω_0 and μ inside this region, no inner DRC exists. Numerical validation of this finding is reported below at the end of this section.

To get a useful analytical expression for the extremum of the bifurcation curve corresponding to the jump-up frequencies, a further assumption is introduced and the mass of the attachment is considered negligible respect to that of the primary system. As such, Eq. (9) reduces to

$$\gamma_u\big|_{\zeta_s=\zeta=\mu=0} = \frac{16\left(\Omega^2-1\right)^2\left(\Omega^2-\Omega_0^2\right)^3}{81\Omega^4}, \tag{18}$$

which is differentiated once respect to Ω and set to zero yielding

$$\frac{\partial}{\partial\Omega}\gamma_u\bigg|_{\zeta_s=\zeta=\mu=0} = \frac{\left(\Omega^2-1\right)\left(\Omega^2-\Omega_0^2\right)\left(3\Omega^4-\Omega^2-2\Omega_0^2\right)}{\Omega} = 0. \tag{19}$$

The expressions for the real positive solutions of Eq. (19) corresponding to the system parameters as reported in the caption of Fig. 10, are $\Omega = 1$, $\Omega = \sqrt{1/6+1/6\sqrt{1+24\Omega_0^2}} \approx 1.14972$ and $\Omega = \Omega_0 = 1.4$. Equation (18) is also plotted in Fig. 10 for comparison as a continuous dashed line. It is noted that for $\Omega = 1$ there is a relative maximum point C_2, for $\Omega \approx 1.14972$ there is a relative minimum point C_3, and for $\Omega = 1.4$ there is an inflexion point C_4. These values are also reported in Table 1 and the corresponding points are shown in Fig. 10.

For the values of the system parameters used to plot Fig. 10 and to report on Table 1, the following may be observed. As highlighted earlier in Section 4, the approximate

expression derived in Eq. (9), in the assumption of light damping, appears to be a good approximation of Eq. (8). In particular, the error in estimating the value of frequency corresponding to the minimum is less than 0.1% , and the value of the minimum in terms of γ is affected by an error of less than 1% .

The approximate expression given in Eq. (18), derived in the further assumption of light mass ratio, does not appear as a good approximation of Eq. (8), as already mentioned in Section 4 when commenting on the effect of the mass ratio on the bifurcation curves in Fig. 4. However, while the error in estimating the minimum in terms of γ is well above 80% , the error in estimating the value of the frequency corresponding to the minimum is only about 2%. In this paper, it is then considered that the following expression

$$\Omega^* = \sqrt{\frac{1}{6} + \frac{1}{6}\sqrt{1+24\Omega_0^2}}\,, \tag{20}$$

derived from Eq. (18) is a good approximation for the frequency corresponding to the extremum point responsible for the appearance of an inner DRC.

The corresponding value for γ is determined by substituting Eq. (20) into Eq. (9) to get

$$\gamma^* = -\frac{16\left(2\left(1+\sqrt{1+24\Omega_0^2}\right)+3\Omega_0^2\left(-9+\mu+\sqrt{1+24\Omega_0^2}+\mu\sqrt{1+24\Omega_0^2}\right)\right)^3}{2187\left(1+\sqrt{1+24\Omega_0^2}\right)^2\left(-5+\mu+\sqrt{1+24\Omega_0^2}+\mu\sqrt{1+24\Omega_0^2}\right)}\,. \tag{21}$$

Thus, provided that the values of Ω_0 and μ are outside the grey-shaded region in Fig. 11, the value of γ for which an inner DRC begins to emerge in the FRC is given by Eq. (21).

By analysing the sign of Eq. (21) and its relation to Ω_0 and μ, it results that γ^* is negative when the pair of values (Ω_0, μ) corresponds to a point belonging to the large white region on the right in Fig. 11, and it is positive when the pair of values (Ω_0, μ) corresponds to a point belonging to the small white region on the bottom left in Fig. 11. This means that for a system with a hardening spring characteristics, the inner DRC manifests for low values of the mass ratio and stiffness ratio, but for a system with a softening spring characteristics, the range of values that the mass and stiffness ratio may achieve for an inner DRC to emerge is much larger.

The validation of Fig. 11 and Eq. (21) is achieved by varying the values of Ω_0 and μ in the full range [0, 2] with an increment of 0.05 and calculating the extremum point of Eq. (8) numerically. The relative error introduced by using Eq. (21) is then calculated and plotted in Fig. 12 as a different marker, depending on the error achieved: for red circles the relative error is less than 15% and greater than 10%, for yellow diamonds the relative error is less than 10% and greater than 5%, and for green squares the relative error is less than 5%. The non-existence of an extremum point in Eq. (8) corresponds to a no-solution for the specific combination of mass and stiffness ratios, i.e. no marker in Fig. 12. The no-solution region computed numerically in Fig. 12 corresponds to the analytical expression reported in the graph of Fig. 11, which is also plotted in Fig. 12 as a thick dashed line.

It is observed that the approximation introduced by Eq. (21) is about 15% for combinations of values of Ω_0 and μ very close to the boundary of the grey-shaded region in Fig. 11, but is decreases dramatically beyond that boundary, so that the

approximation introduced by Eq. (21) is below 5% for the majority of the combinations of Ω_0 and μ.

8 CONCLUSIONS

This paper presents an investigation on the appearance of isolated detached resonance curves inside the main continuous frequency response curve of nonlinear coupled oscillators. A general relation between the frequency response curve and the bifurcation curve is emphasized, as also discussed in [6], and that is used to study the formation of detachments. The specific case considered in the paper, i.e. that of a two degree-of-freedom nonlinear system with cubic stiffness nonlinearity, allowed the derivation of approximate analytical expressions, which let a further insight on the effects of the main system parameters. Close-form expressions for the amplitude-frequency equations and detachments are derived by the harmonic balance method and verified by direct numerical integration of the equations of motion. Analytical expressions for the bifurcation curves, which give indication of multivaluedness in the frequency response, are also determined as implicit functions of the nonlinearity and the excitation frequency. The effect of the system parameters on the bifurcation curves is illustrated and discussed. It is remarked that points on the bifurcation curves correspond to the jump-up or jump-down frequencies in the frequency response curve. It is further observed that an isolated detached resonance curve appears when the bifurcation curve presents an extremum point. This condition is then investigated in the assumption of light damping, which is shown not to affect significantly the jump-up frequencies of the system, and focus is thus devoted to inner detachments appearing in the frequency response curve of the amplitude

of the relative displacement between the primary and secondary mass. It is shown that those detachments are formed when two consecutive jump-up frequencies are present. Approximate analytical expressions are determined which shed light on (i) the combination of mass and frequency ratio affecting the appearance of isolated detachments, (ii) the relation between such combination of parameters and the sign of the nonlinearity, related to the hardening/softening characteristics of the nonlinear spring, (iii) the limiting value for the nonlinearity beyond which a closed detachment emerges inside the main continuous frequency response curve.

REFERENCES

[1] A.H. Nayfeh, D.T. Mook, Nonlinear Oscillations, Wiley, New York, 1979.

[2] Y. Starosvetsky, O.V. Gendelman, Vibration absorption in systems with a nonlinear energy sink: Nonlinear damping. Journal of Sound and Vibration 324 (2009) 916-939.

[3] Y. Starosvetsky, O.V. Gendelman, Dynamics of a strongly nonlinear vibration absorber coupled to a harmonically excited two-degree-of-freedom system. Journal of Sound and Vibration 312 (2008) 234-256.

[4] P. Malatkar, A.H. Nayfeh, Steady-state dynamics of a linear structure weakly coupled to an essentially nonlinear oscillator. Nonlinear Dynamics 47 (2007) 167-179.

[5] N.A. Alexander, F. Schilder, Exploring the performance of a nonlinear tuned mass damper. Journal of Sound and Vibration 319 (2009) 445-462.

[6] T. Detroux, L. Renson, L. Masset, G. Kerschen, The harmonic balance method for bifurcation analysis of large-scale nonlinear mechanical systems. Computer Methods in Applied Mechanics and Engineering 296 (2015) 18-38.

[7] R.J. Kuether, L. Renson, T. Detroux, C. Grappasonni, G. Kerschen, M.S. Allen, Nonlinear normal modes, modal interactions and isolated resonance curves. Journal of Sound and Vibration 351 (2015) 299-310.

[8] C. Duan, R. Singh, Isolated sub-harmonic resonance branch in the frequency response of an oscillator with slight asymmetry in the clearance. Journal of Sound and Vibration 314 (2008) 12-18.

[9] M. Elmegård, F. Schilder, H.M. Osinga, J. Starke, J.J. Thomsen, Bifurcation analysis of a smoothed model of a forced impacting beam and comparison with an experiment. Nonlinear Dynamics, 77 (2014) 951-966.

[10] G. Gatti, M.J. Brennan, On the effects of system parameters on the response of a harmonically excited system consisting of weakly coupled nonlinear and linear oscillators. Journal of Sound and Vibration 330 (2011) 4538-4550.

[11] G. Gatti, M.J. Brennan, I. Kovacic, On the interaction of the responses at the resonance frequencies of a nonlinear two degree-of-freedom system. Physica D: Nonlinear Phenomena 239 (2010) 591-599.

[12] M.J. Brennan, G. Gatti, The characteristics of a nonlinear vibration neutralizer. Journal of Sound and Vibration 331(2012) 3158-3171.

[13] K. Worden, On jump frequencies in the response of the Duffing oscillator. Journal of Sound and Vibration 198 (1996) 522-525.

[14] M.J. Brennan, I. Kovacic, A. Carrella, T.P. Waters, On the jump-up and jump-down frequencies of the Duffing oscillator. Journal of Sound and Vibration 318 (2008) 1250-1261.

[15] A.H. Nayfeh, B. Balachandran, Applied Nonlinear Dynamics, Wiley, New York, 1995.

[16] G. Gatti, I. Kovacic, M.J. Brennan, On the response of a harmonically excited two degree-of-freedom system consisting of a linear and a nonlinear quasi-zero stiffness oscillator. Journal of Sound and Vibration 329 (2010) 1823-1835.

[17] G.A. Korn, T.M. Korn, Mathematical Handbook for Scientists and Engineers, McGraw-Hill, NewYork, 1961.

Appendix A

This Appendix is aimed at giving some more details on the steps used to derive Eqs. (3), (4) and (6) from the harmonic balance method.

To apply the harmonic balance method, the displacements of the system are assumed in the form of

$$y_s \approx Y_s \cos\left(\Omega\tau + \varphi_s\right) \tag{A.1}$$

$$w \approx W \cos\left(\Omega\tau + \varphi\right) \tag{A.2}$$

and these are first substituted into Eq. (2b). Since a first-order approximation is adopted, it is assumed that $\cos(\square)^3 = \frac{1}{4}\cos(3\square) + \frac{3}{4}\cos(\square) \approx \frac{3}{4}\cos(\square)$. Trigonometric addition and subtraction formulas are then used to separate the terms $\cos\left(\Omega\tau\right)$ and $\sin\left(\Omega\tau\right)$, and their coefficients are equated correspondingly to obtain the following two equations

$$-\Omega^2 W\cos\left(\varphi\right) - 2\zeta\Omega W\sin\left(\varphi\right) + \Omega_0^2 W\cos\left(\varphi\right) + \frac{3}{4}\gamma W^3\cos\left(\varphi\right) = -\Omega^2 Y_s\cos\left(\varphi_s\right) \tag{A.3}$$

$$\Omega^2 W\sin\left(\varphi\right) - 2\zeta\Omega W\cos\left(\varphi\right) - \Omega_0^2 W\sin\left(\varphi\right) - \frac{3}{4}\gamma W^3\sin\left(\varphi\right) = \Omega^2 Y_s\sin\left(\varphi_s\right) \tag{A.4}$$

To get rid of the phases, Eqs. (A.3) and (A.4) are squared and added to get Eq. (3).

To retrieve a first set of equations for the phases, Eq. (A.4) is multiplied by $-j = -\sqrt{-1}$ and added to Eq. (A.3). By using the Euler's formula and equating the coefficients of the

real and imaginary parts of the resulting equation, the following expressions for the phase $\Delta\varphi = \varphi_s - \varphi$ are obtained

$$\cos\left(\Delta\varphi\right) = \frac{-W}{\Omega^2 Y_s}\left(\Omega_0^2 - \Omega^2 + \frac{3}{4}\gamma W^2\right) \tag{A.5}$$

$$\sin\left(\Delta\varphi\right) = \frac{-2\zeta W}{\Omega\ Y_s} \tag{A.6}$$

In a second step, Eqs. (A.1) and (A.2) are substituted into Eq. (2a), and using an approach similar to that described above, Eq. (4) is obtained, as well as the following expressions for the phase φ_s

$$\cos\left(\varphi_s\right) = Y_s\left(1 - \Omega^2\left(1 + \mu\right)\right) + \Omega^2 \mu W \cos\left(\Delta\varphi\right) \tag{A.7}$$

$$\sin\left(\varphi_s\right) = -2\zeta_s \Omega Y_s + \Omega^2 \mu W \sin\left(\Delta\varphi\right) \tag{A.8}$$

In the third step, since it is assumed that $y = y_s - w \approx Y\cos\left(\Omega\tau + \varphi\right)$, its amplitude is given by Eq. (6), while the expressions for its phase are given below as

$$\cos\left(\varphi\right) = \cos\left(\Delta\varphi\right)\cos\left(\varphi_s\right) + \sin\left(\Delta\varphi\right)\sin\left(\varphi_s\right) \tag{A.9}$$

$$\sin\left(\varphi\right) = \cos\left(\Delta\varphi\right)\sin\left(\varphi_s\right) - \sin\left(\Delta\varphi\right)\cos\left(\varphi_s\right) \tag{A.10}$$

Figure Captions List

Fig. 1 Model of the two DOF nonlinear system.

Fig. 2 Effect of ζ_s on the bifurcation curves for $\mu = 0.15, \zeta = 0.01$, $\zeta_s = 0.005$ (thick dot lines), $\zeta_s = 0.01$ (thick dash-dot lines), $\zeta_s = 0.03$ (thick dash lines) and (a) $\Omega_0 = 0.3$, (b) $\Omega_0 = 1.3$. The thin solid line represents the bifurcation curve for $\zeta_s = \zeta = 0$.

Fig. 3 Effect of ζ on the bifurcation curves for $\mu = 0.15, \zeta_s = 0.01, \zeta = 0.005$ (thick dot lines), $\zeta = 0.01$ (thick dash-dot lines), $\zeta = 0.03$ (thick dash lines), and (a) $\Omega_0 = 0.3$, (b) $\Omega_0 = 1.3$. The thin solid line represents the bifurcation curve for $\zeta_s = \zeta = 0$.

Fig. 4 Effect of μ on the bifurcation curves for $\zeta_s = \zeta = 0.01$, $\mu = 0.01$(thick dot lines), $\mu = 0.1$ (thick dash-dot lines), $\mu = 1.3$ (thick dash lines), and (a) $\Omega_0 = 0.3$, (b) $\Omega_0 = 1.3$. The thin solid lines represent the corresponding bifurcation curves for $\zeta_s = \zeta = 0$.

Fig. 5 Effect of Ω_0 on the bifurcation curves for $\zeta_s = \zeta = 0.01$, $\Omega_0 = 0.3$ (thick dot lines), $\Omega_0 = 0.7$ (thick dash-dot lines), $\Omega_0 = 1.4$ (thick dash lines), and (a) $\mu = 0.1$, (b) $\mu = 1.3$. The thin solid lines represent the corresponding bifurcation curves for $\zeta_s = \zeta = 0$.

Fig. 6 Three-dimensional plot illustrating the relationship between the bifurcation curves and the FRCs for $\zeta_s = \zeta = 0.01$, $\mu = 0.05$, $\Omega_0 = 0.2$

and (a) $\gamma = 0.2$, (b) $\gamma = 0.008$, (c) $\gamma = 4\times10^{-4}$. On the $\Omega-\gamma$ plane, γ_u is indicated by the upper magenta thin solid line, γ_d by the lower green one. On the $\Omega-W$ plane, the FRC is plotted with the stable solutions (blue solid line) and the unstable solutions (red/magenta dashed line). The intersections between the $\Omega-W$ plane containing the FRC and the bifurcation curves on the $\Omega-\gamma$ plane indicate the jump frequencies. (For interpretation of the references to colour in this figure legend, the reader is referred to the web version of this article)

Fig. 7 Three-dimensional plot illustrating the relationship between the bifurcation curves and the FRCs for $\zeta_s = \zeta = 0.01$, $\mu = 0.05$, $\Omega_0 = 1.4$ and (a) $\gamma = -0.06$, (b) $\gamma = -0.006$, (c) $\gamma = -0.0001$. On the $\Omega-\gamma$ plane, γ_u is indicated by the lower magenta thin solid line, γ_d by the upper green one. On the $\Omega-W$ plane, the FRC is plotted with the stable solutions (blue solid line) and the unstable solutions (red/magenta dashed line). The intersections between the $\Omega-W$ plane containing the FRC and the bifurcation curves on the $\Omega-\gamma$ plane indicate the jump frequencies. (For interpretation of the references to colour in this figure legend, the reader is referred to the web version of this article)

Fig. 8 FRCs of the non-dimensional displacement amplitude (a) W, (b) Y_s and (c) Y, for $\zeta_s = \zeta = 0.01$, $\mu = 0.05$, $\Omega_0 = 0.2$ and $\gamma = 0.008$. Stable analytical solutions (blue solid lines), unstable analytical solutions (red/magenta dashed lines), numerical solutions (black circles). (For interpretation of

the references to colour in this figure legend, the reader is referred to the web version of this article)

Fig. 9 FRCs of the non-dimensional displacement amplitude (a) W, (b) Y_s and (c) Y, for $\zeta_s = \zeta = 0.01$, $\mu = 0.05$, $\Omega_0 = 1.4$ and $\gamma = -0.006$. Stable analytical solutions (blue solid lines), unstable analytical solutions (red dashed lines), numerical solutions (black circles). (For interpretation of the references to colour in this figure legend, the reader is referred to the web version of this article)

Fig. 10 Bifurcation curve relative to the jump-up frequencies for $\zeta_s = \zeta = 0.01$, $\Omega_0 = 1.4$ and $\mu = 0.1$ based on Eq. (8) (magenta solid line), on the approximation for $\zeta_s = \zeta = 0$ of Eq. (9) (dotted line), and on the approximation for $\zeta_s = \zeta = \mu = 0$ of Eq. (18) (dashed lines). Extrema and inflexion points are labeled as A (black dots), B (empty squares) and C (filled diamonds) for each of the three curves, respectively, and listed in Table 1.

Fig. 11 Regions of the existence of a DRC in the $\Omega_0 - \mu$ plane. For a pair of values of the frequency and mass ratio inside the grey-shaded region there is no DRC. In the white regions, DRC are predicted in the FRC for hardening and softening spring characteristics as labelled.

Fig. 12 Validation of Fig. 11 showing the relative error between the limiting value for nonlinearity given by the approximate expression in Eq. (21), and the value of the local extremum of the bifurcation curve in Eq. (8) for the

jump-up frequencies computed numerically, for different combination of Ω_0 and μ in the range [0, 2]. Relative error less than 15% and greater than 10% (red circles), relative error less than 10% and greater than 5% (yellow diamonds), and relative error less than 5% (green squares). (For interpretation of the references to colour in this figure legend, the reader is referred to the web version of this article)

Table Caption List

Table 1 Frequencies corresponding to extrema and inflexion points of the bifurcation curve for the jump-up frequencies given in Eq. (8) and its approximations given in Eqs. (9) and (18), for $\zeta_s = \zeta = 0.01$, $\omega_0 = 1.4$ and $\mu = 0.1$.

Figure 1

Click here to download high resolution image

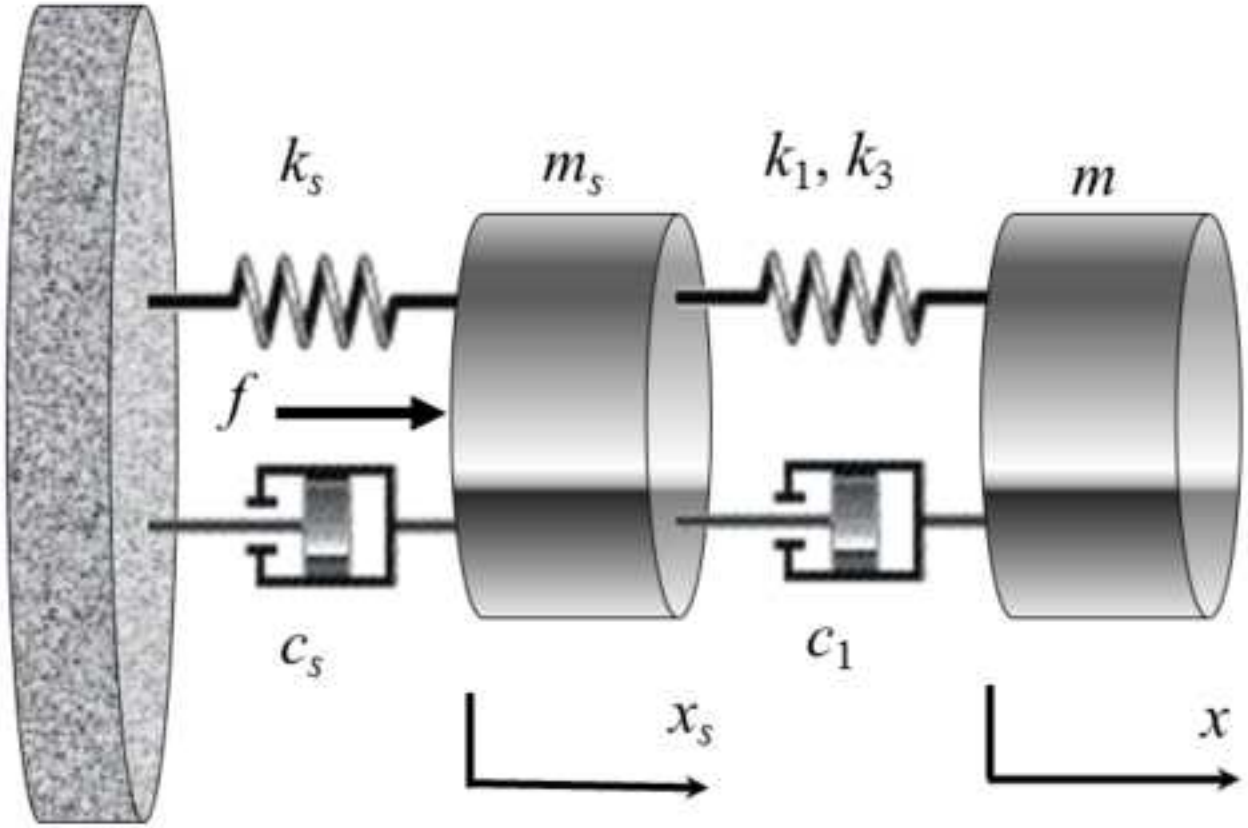

Figure 2ab

Click here to download high resolution image

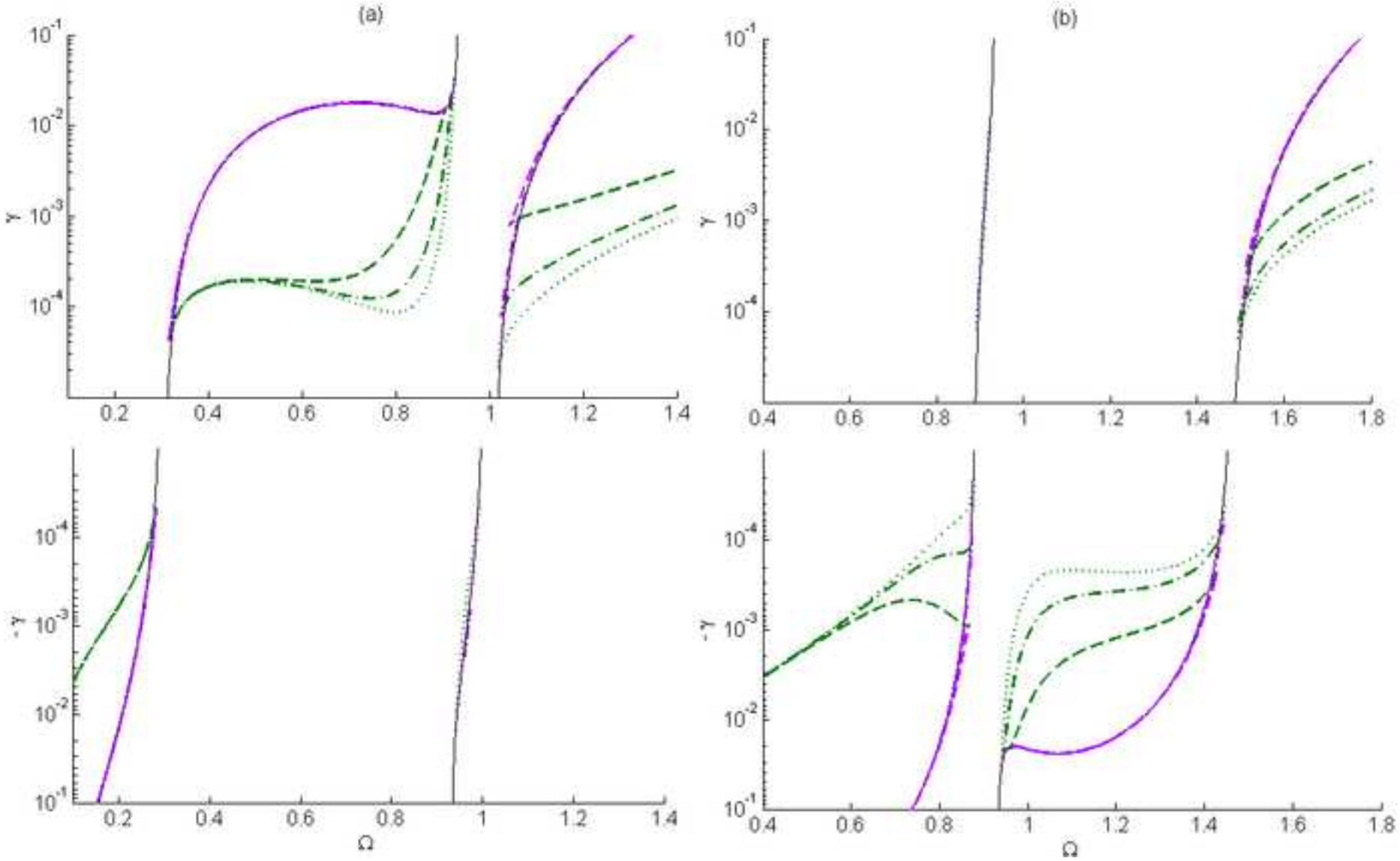

Figure 3ab

Click here to download high resolution image

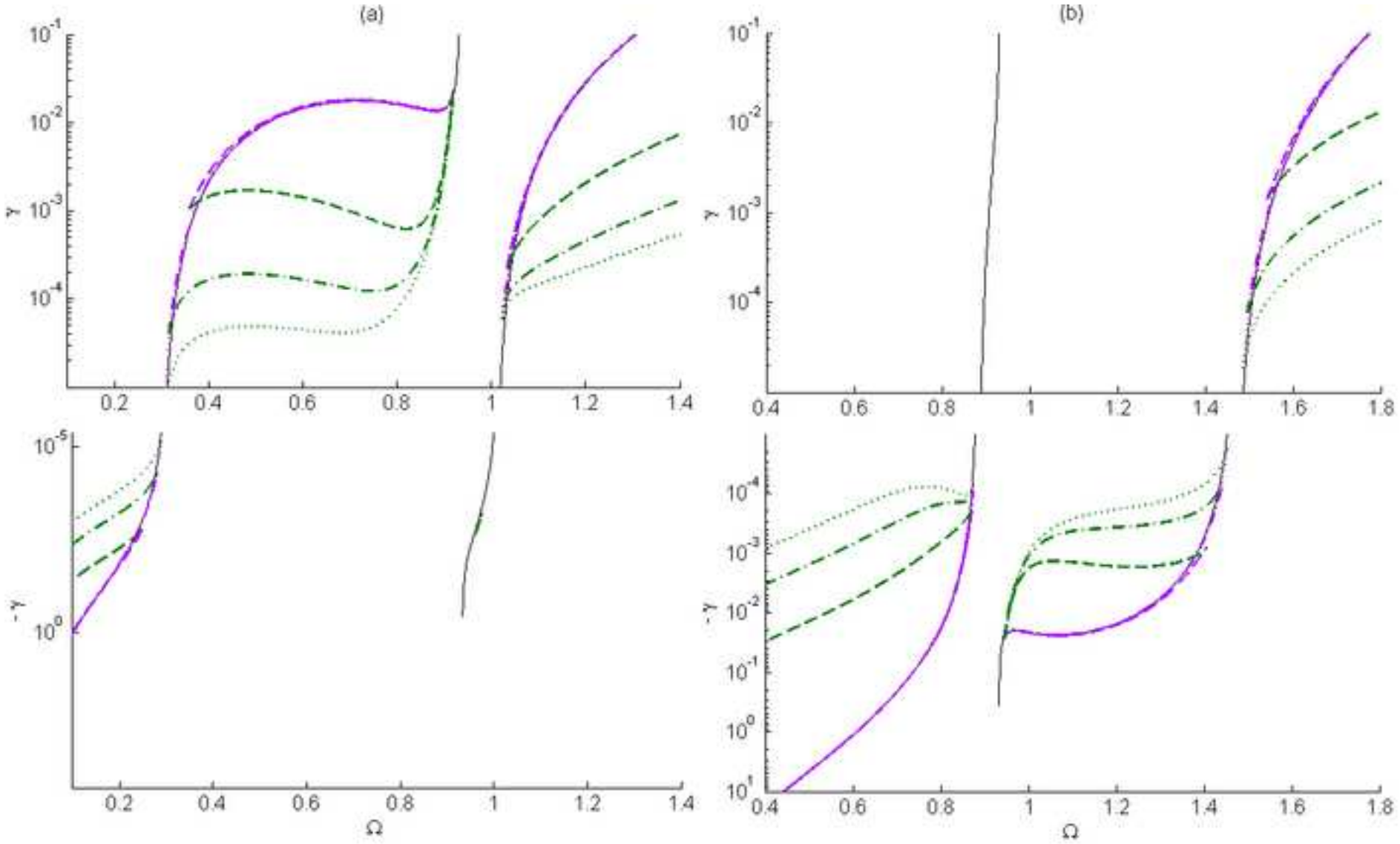

Figure 4ab

Click here to download high resolution image

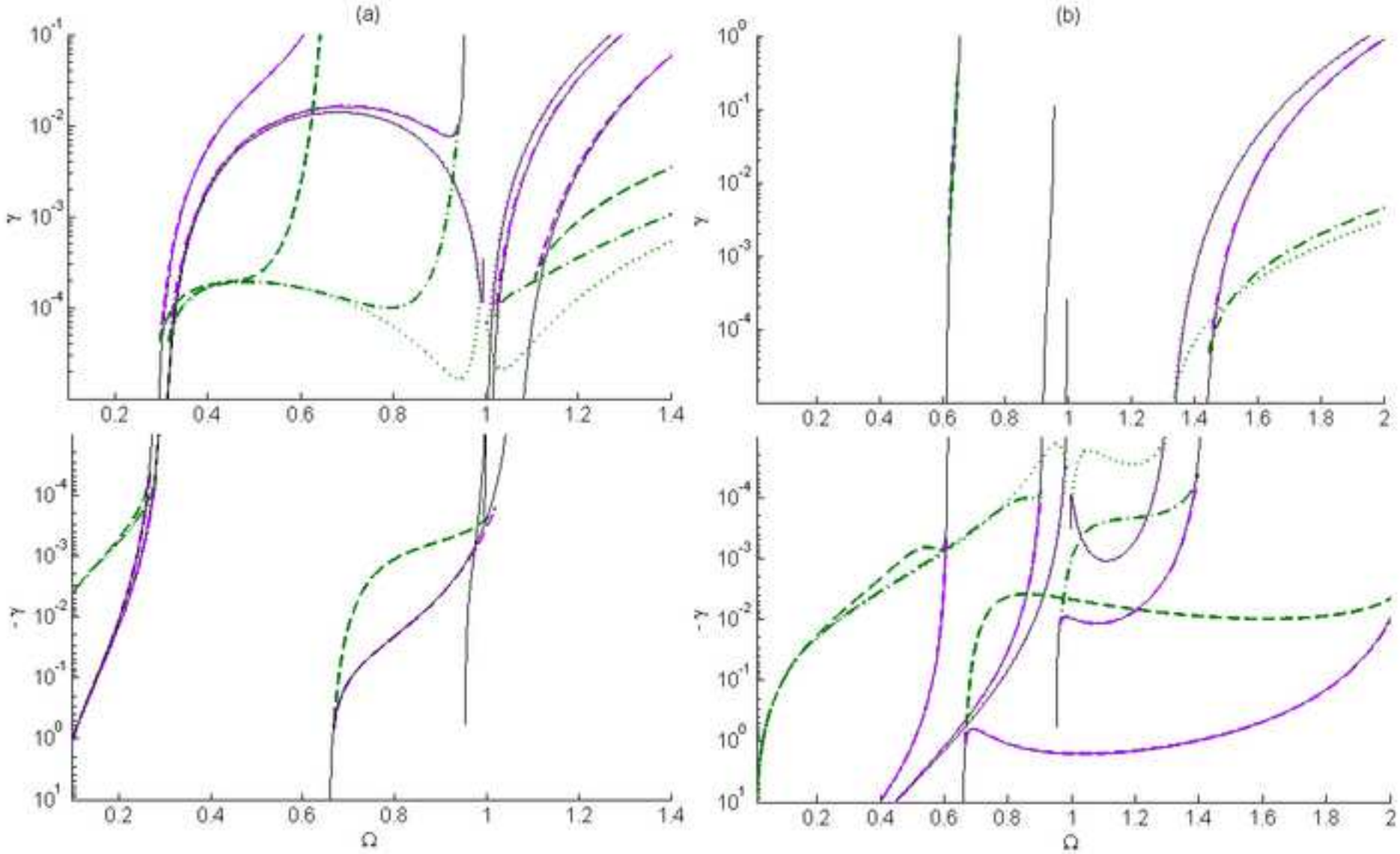

Figure 5ab

Click here to download high resolution image

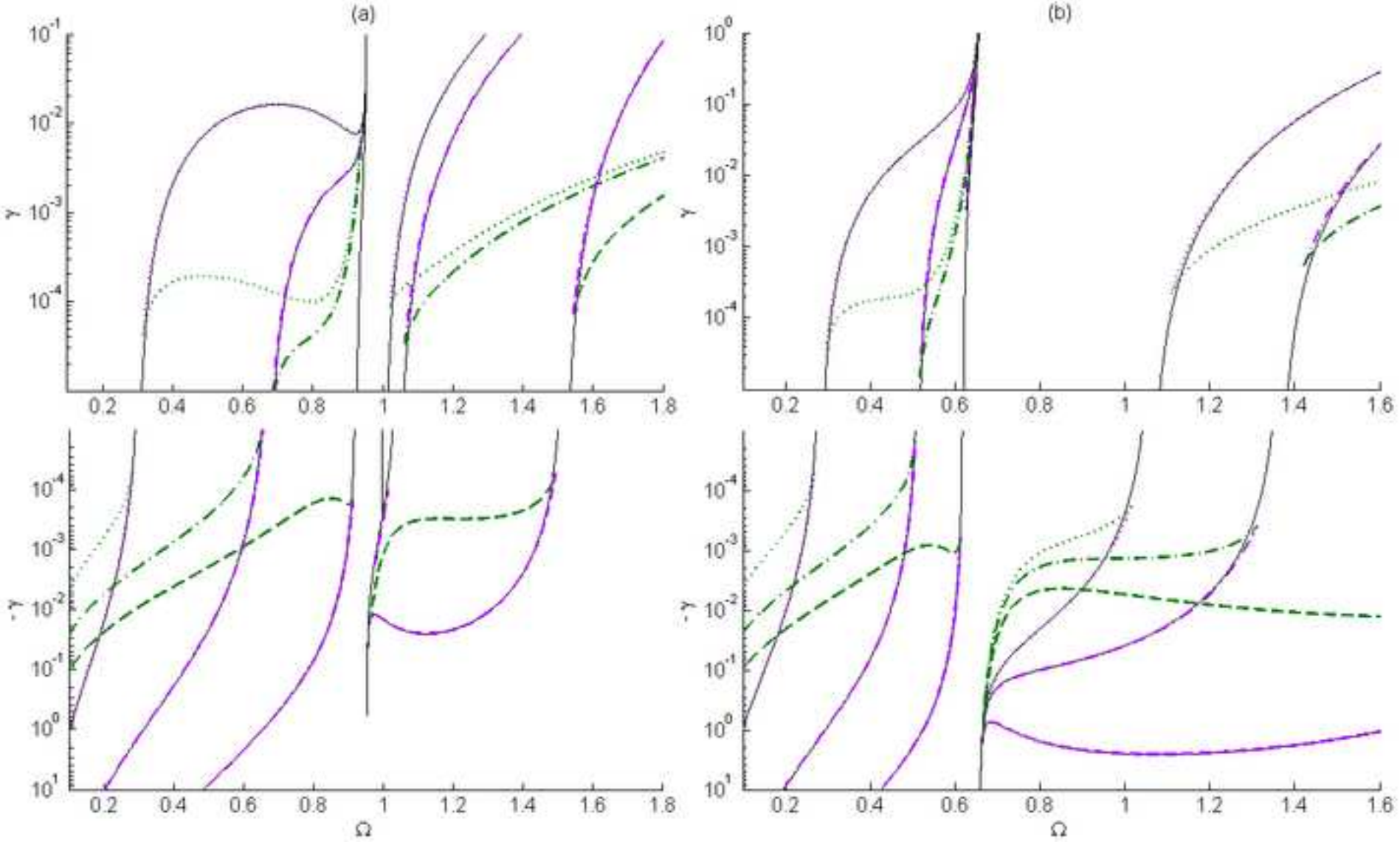

Figure 6abc

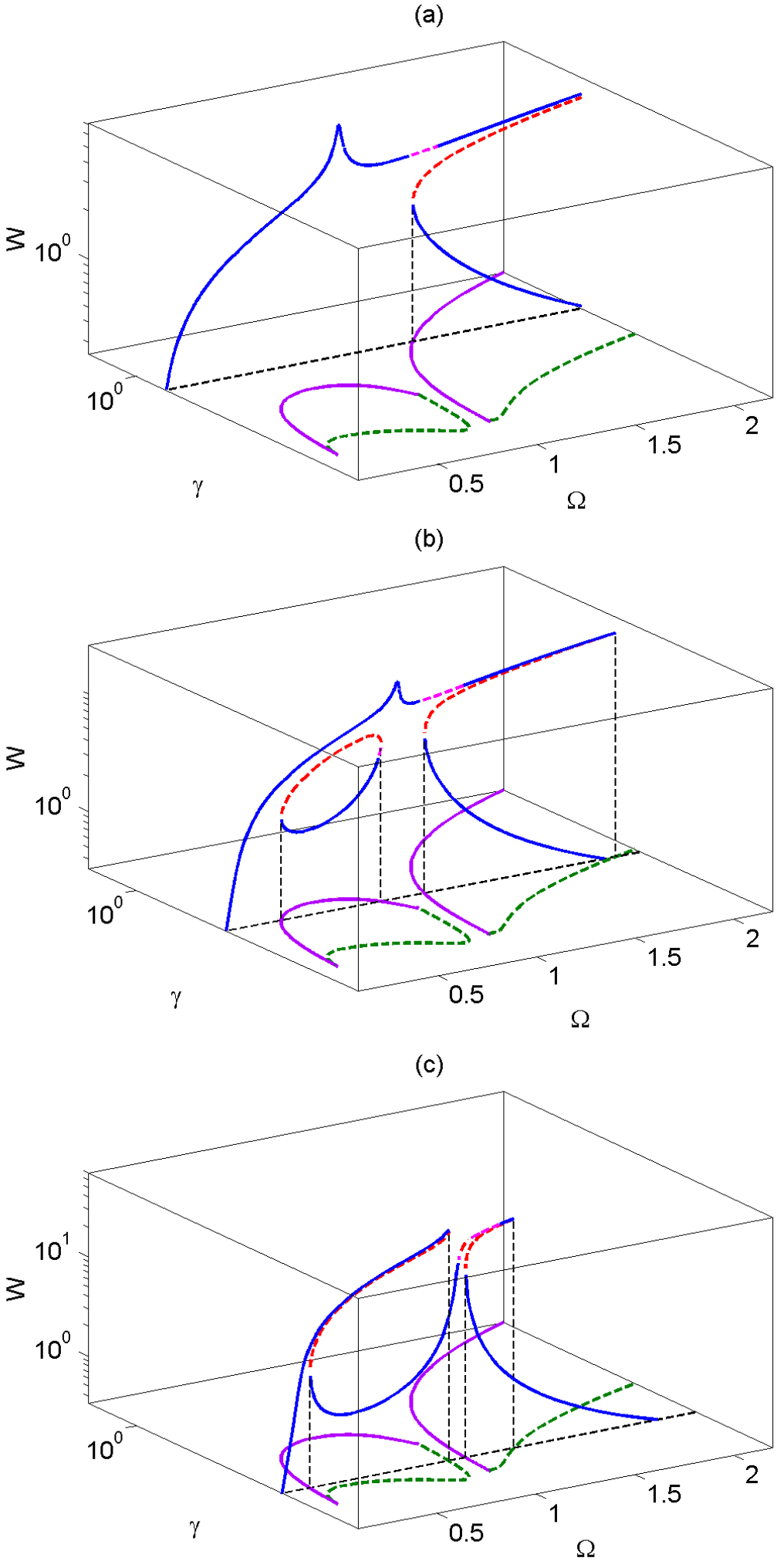
(a)
W
10^0
10^0
γ
0.5
1
1.5
2
Ω
(b)
W
10^0
10^0
γ
0.5
1
1.5
2
Ω
(c)
W
10^1
10^0
10^0
γ
0.5
1
1.5
2
Ω

Figure 7abc

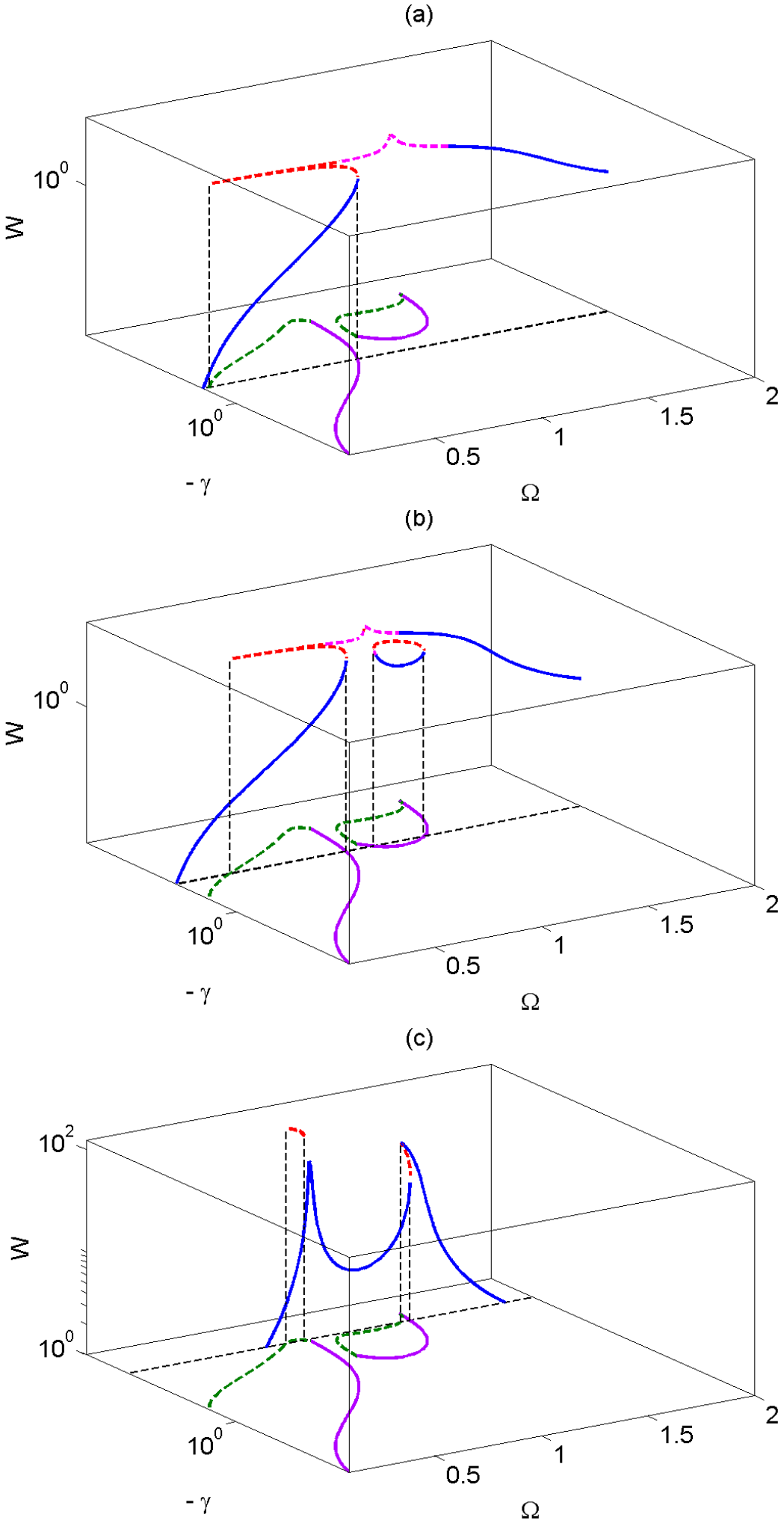
(a)
W
10^0
10^0
- γ
0.5
1
1.5
2
Ω
(b)
W
10^0
10^0
- γ
0.5
1
1.5
2
Ω
(c)
W
10^2
10^0
10^0
- γ
0.5
1
1.5
2
Ω

Figure 8abc

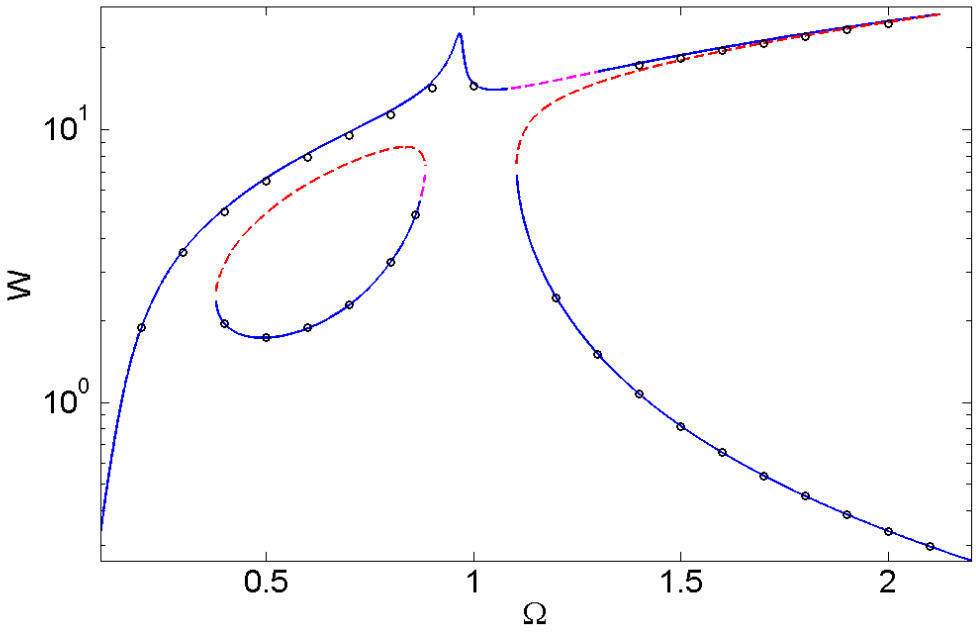

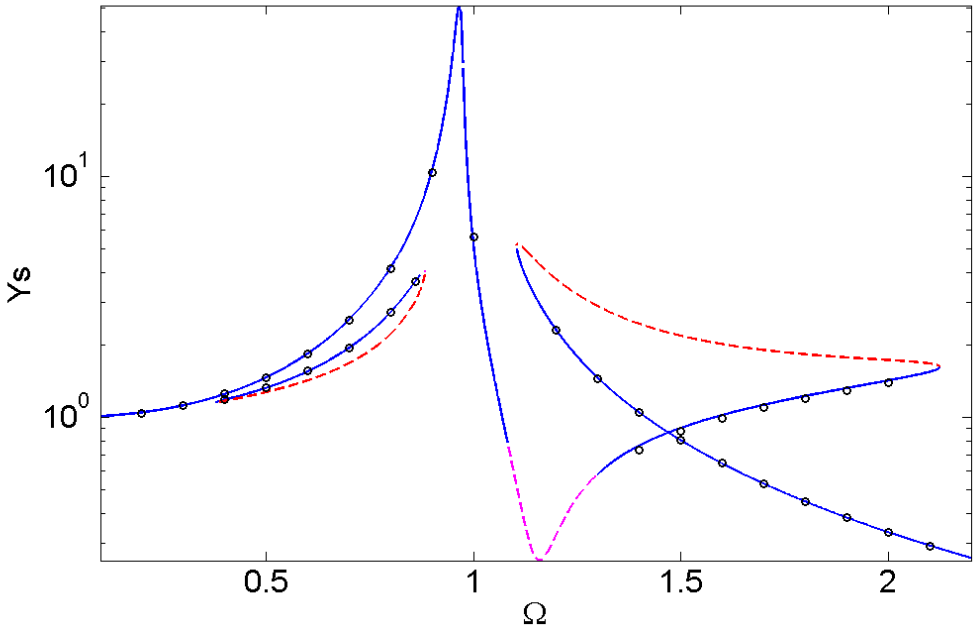

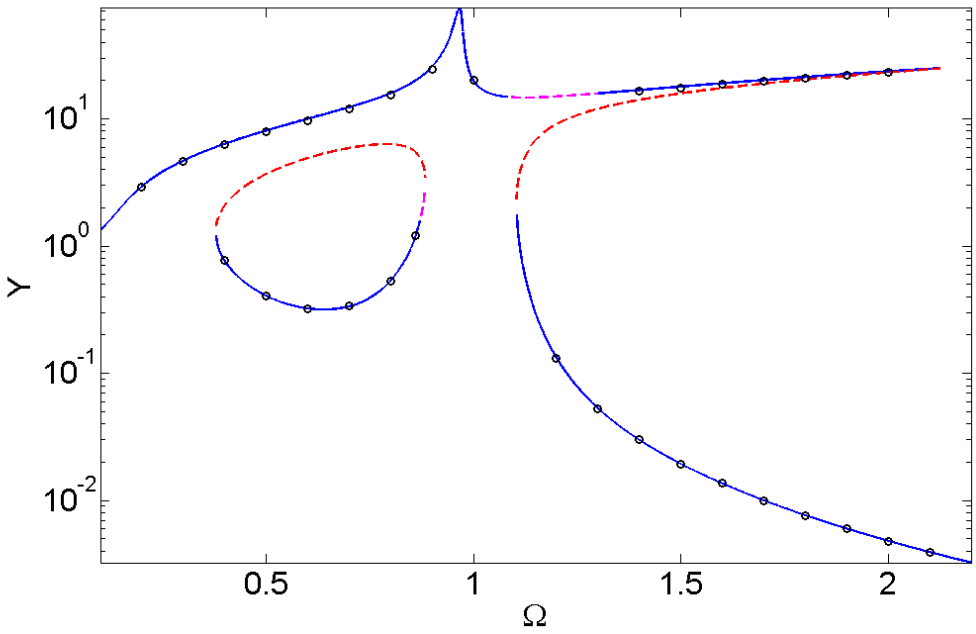

Figure 9abc

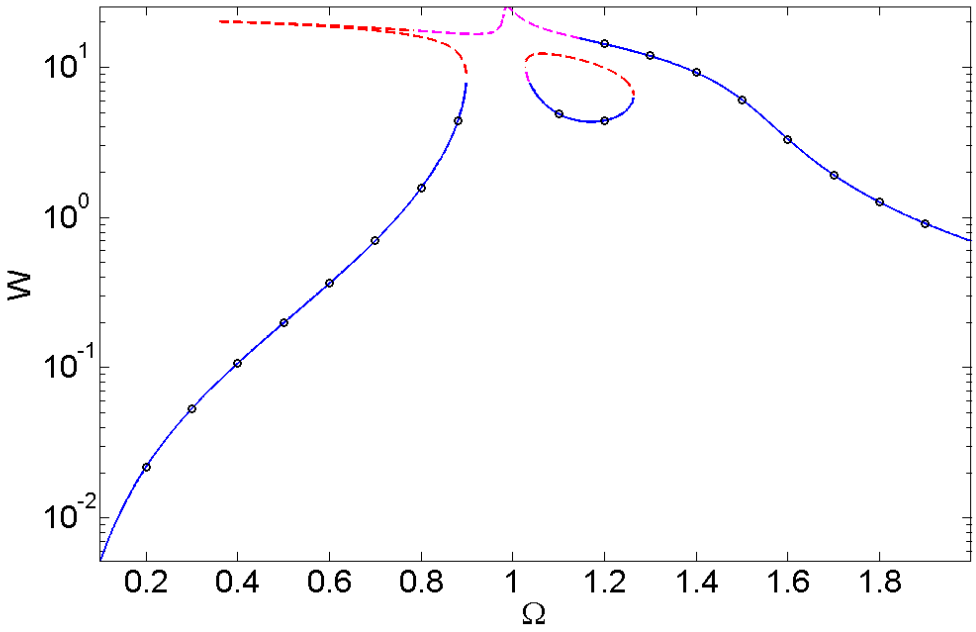
W
10^{1}
10^{0}
10^{-1}
10^{-2}
0.2
0.4
0.6
0.8
1
1.2
1.4
1.6
1.8
Ω

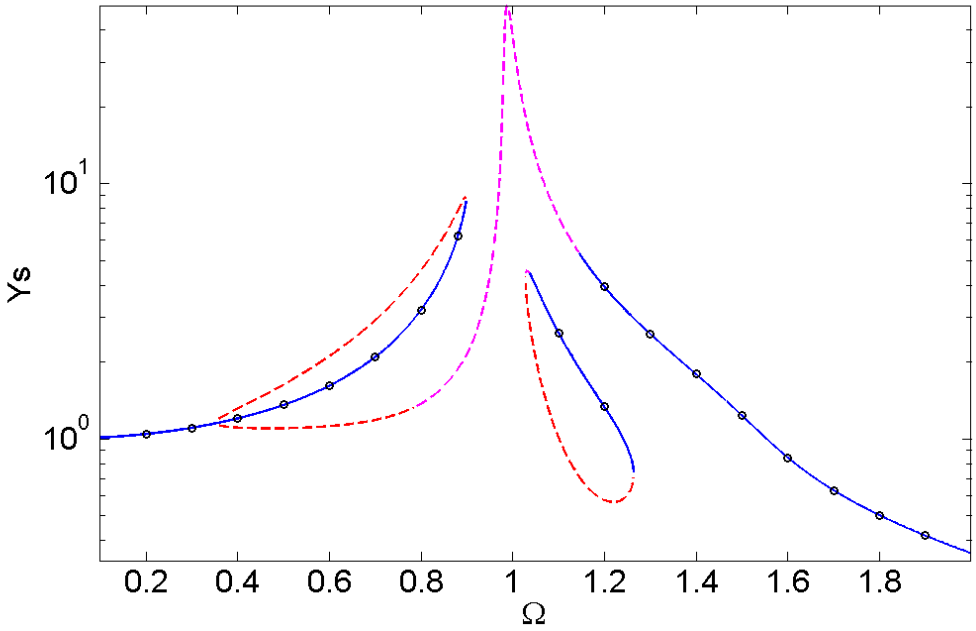
Ys
10^{1}
10^{0}
0.2
0.4
0.6
0.8
1
1.2
1.4
1.6
1.8
Ω

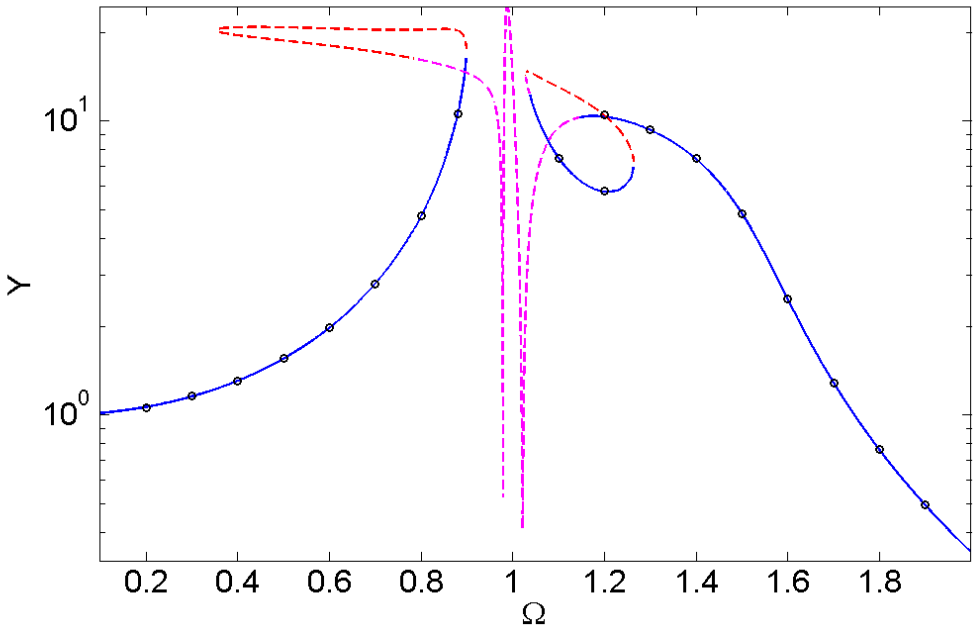
Y
10^{1}
10^{0}
0.2
0.4
0.6
0.8
1
1.2
1.4
1.6
1.8
Ω

Figure 10
Click here to download high resolution image

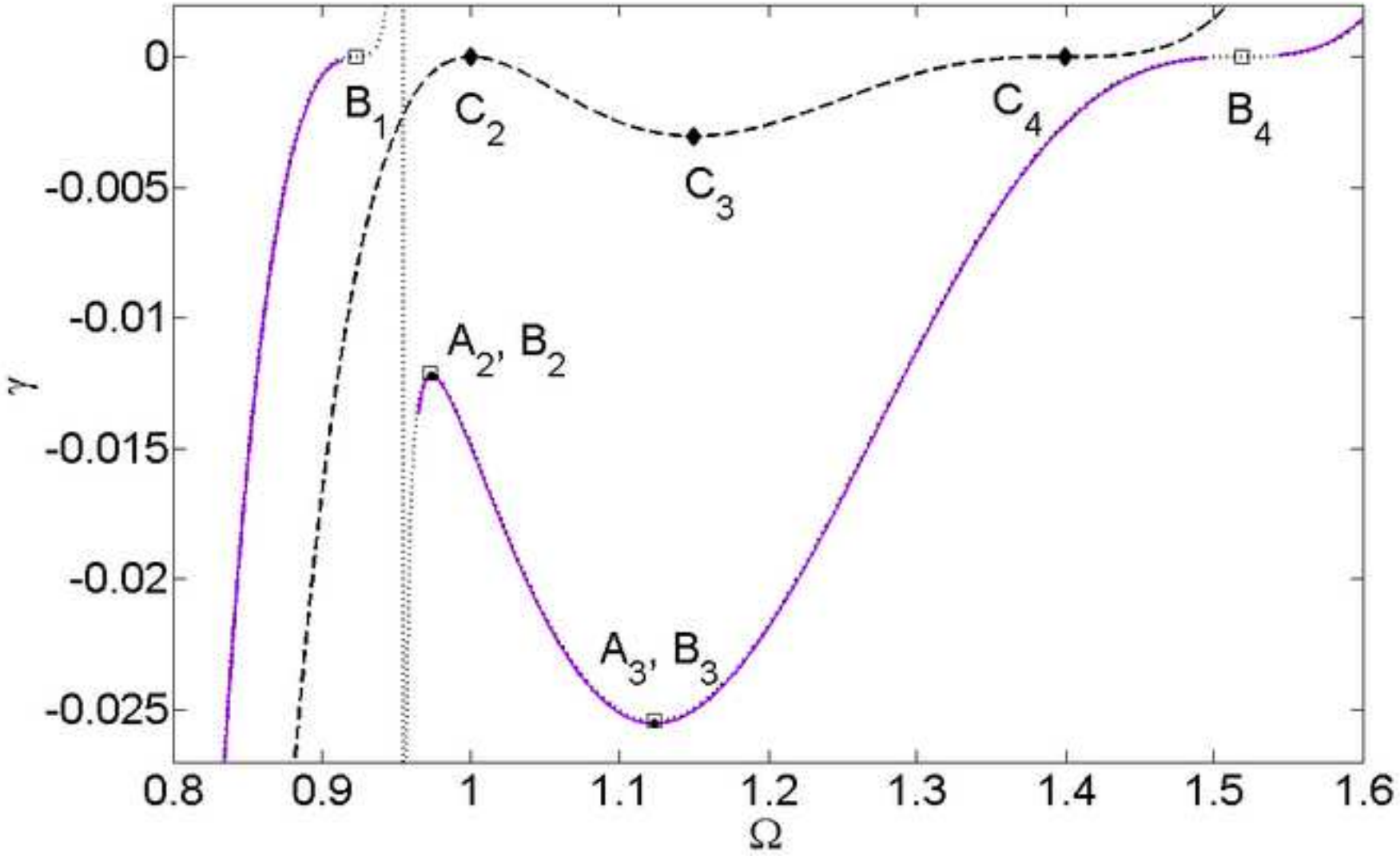

Figure 11
Click here to download high resolution image

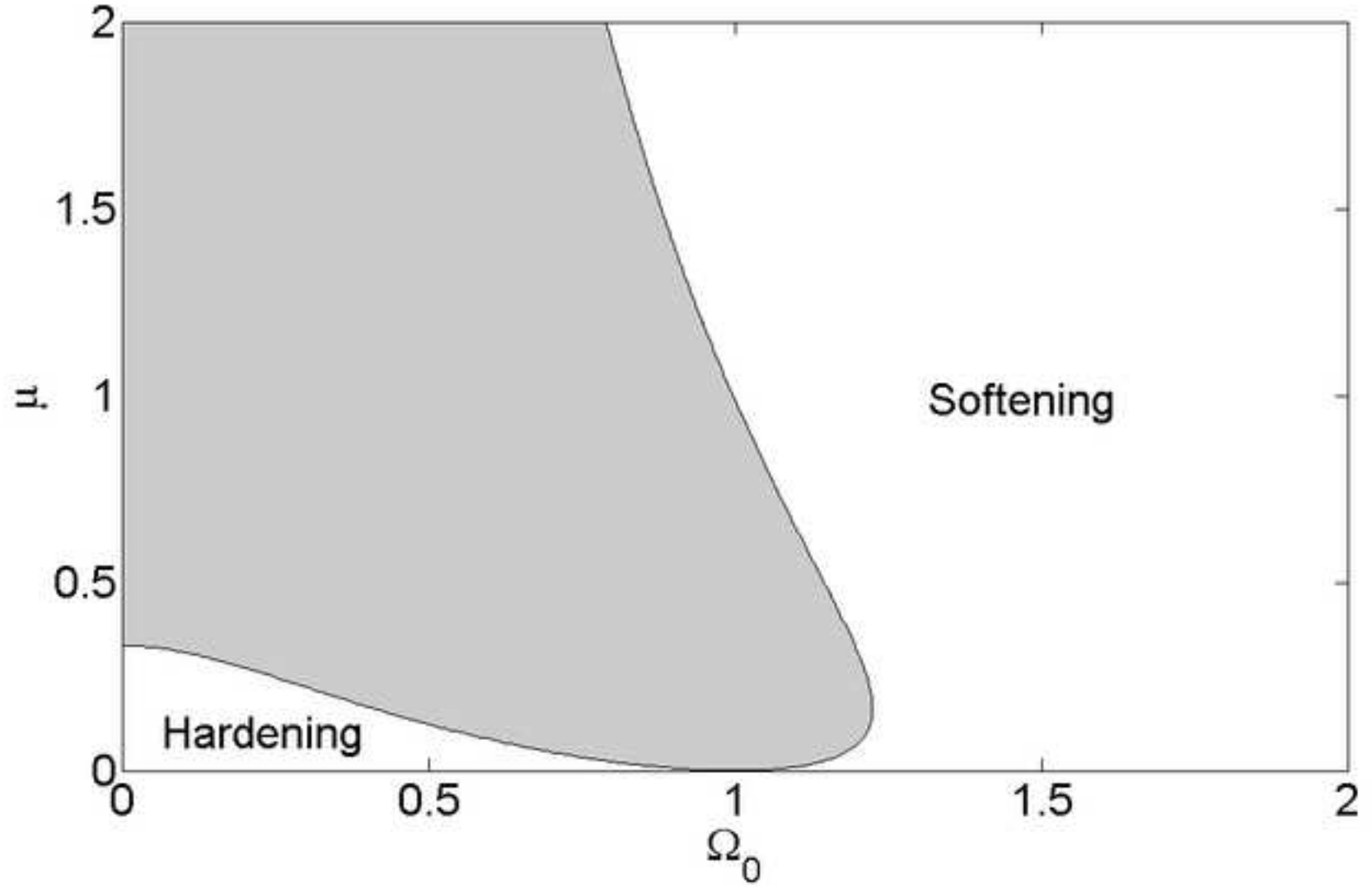

Figure 12

Click here to download high resolution image

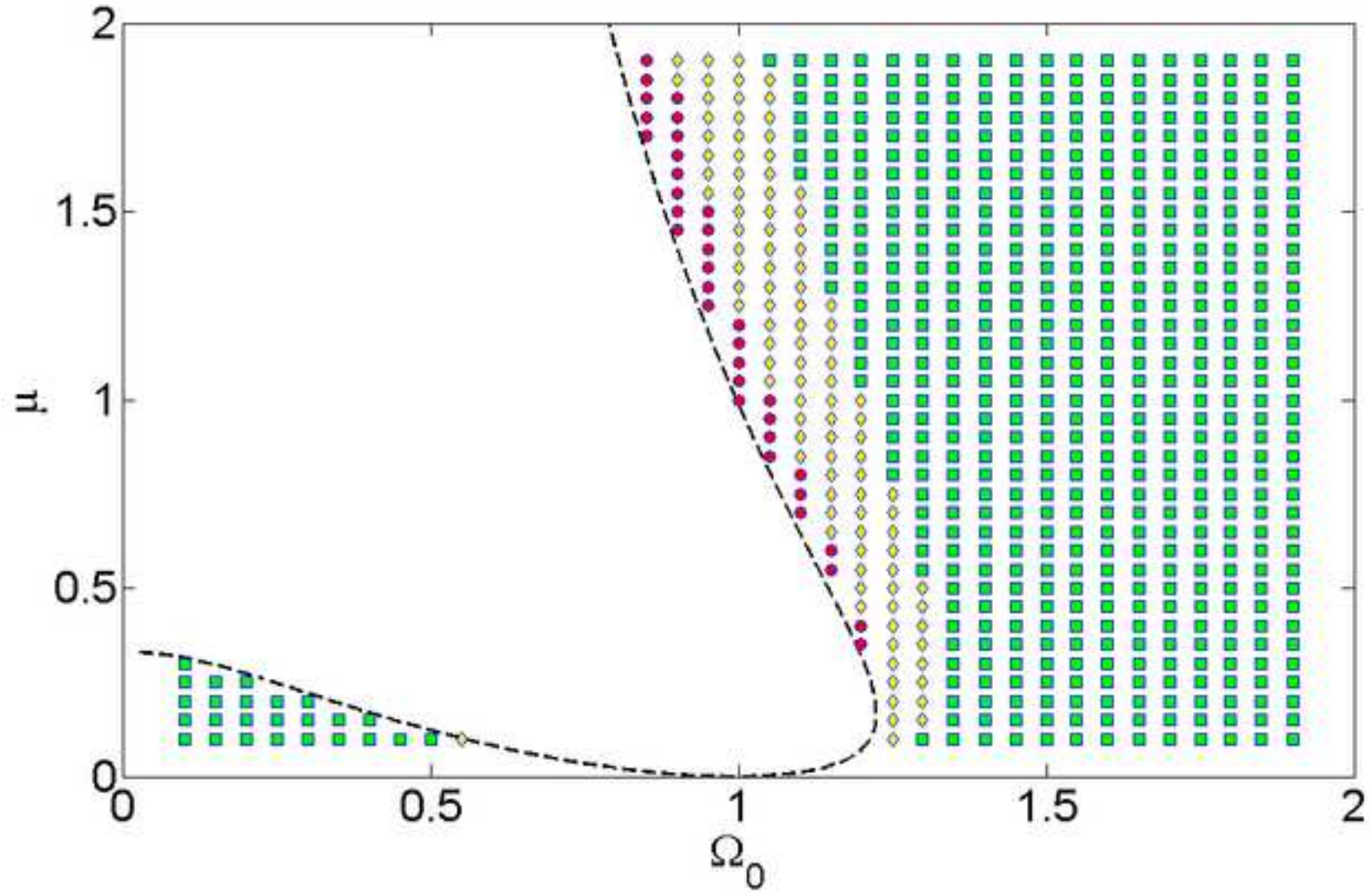

Table 1

	Ω	Point (Type)	Ω	Point (Type)	Ω	Point (Type)	Ω	Point (Type)
Eq. (8a,b)	-	-	0.97316	A_2 (max)	1.12288	A_3 (min)	-	-
Eq. (9)	0.922	B_1 (infl)	0.97286	B_2 (max)	1.12293	B_3 (min)	1.519	B_4 (infl)
Eq. (18)	-	-	1	C_2 (max)	1.14972	C_3 (min)	1.4	C_4 (infl)